A&A 395, 845–851 (2002)
DOI: 10.1051/0004-6361:20021013

Astronomy & Astrophysics

Detection of new optical counterpart candidates to PSR B1951+32 with HST/WFPC2

R. F. Butler, A. Golden, and A. Shearer

National University of Ireland, Galway, University Road, Galway, Ireland

Received 13 September 2001 / Accepted 4 July 2002

Abstract. There remain several definitive γ-ray pulsars that are as yet undetected in the optical regime. A classic case is the pulsar PSR B1951+32, associated with the complex CTB 80 SNR. Previous ground based high speed 2-d optical studies have ruled out candidates to $m_V \sim 24$. Hester (2000a) has reported an analysis of archival HST/WFPC2 observations of the CTB 80 complex which suggest a compact synchrotron nebula coincident with the pulsar's radio position. Performing a similar analysis, we have identified a possible optical counterpart within this synchrotron nebula at $m_V \sim 25.5-26$, and another optical counterpart candidate nearby at $m_V \sim 24.5$. We assess the reality of these counterpart candidates in the context of existing models of pulsar emission.

Key words. stars: pulsars: general – stars: pulsars: individual: PSR B1951+32 – ISM: supernova remnants – ISM: individual objects: CTB 80

1. Introduction

The detection of nonthermal high energy magnetospheric emission from isolated pulsars has remained a non-trivial problem, despite great advances in instrumentation and technological expertise. To date, only 7 optical pulsars have been detected with emission believed to be magnetospherically dominated, and despite considerable effort, only 8 γ-ray pulsars. In contrast to radio emission, which is generally believed to be generated in close proximity to the magnetic poles, no clear theoretical model construct exists as regards the higher energies. The two principal schools of thought place γ-ray emission localised either to the magnetic poles (Daugherty & Harding 1996) or located further out in the magnetosphere (Romani 1996). Considerable problems remain with these two frameworks, in terms of predicted fluxes, spectral indices and light curve morphologies, and it is clear that further work is required on this subject. This is all the more relevant when one attempts to address the growing empirical database of lower energy emission, in particular in the optical regime. A consequence of non-linear processes within the magnetosphere, this synchrotron emission forms a useful constraint with which one can attempt to comprehensively develop a self-consistent theoretical framework. Consequently it is important to try to acquire synchrotron (optical/X-ray) data of known γ-ray pulsars, and so extend this empirical database.

Send offprint requests to: R. F. Butler,
e-mail: ray@physics.nuigalway.ie

The pulsar PSR B1951+32, located within the complex combination supernova remnant (SNR) CTB 80, was first identified as a steep-spectrum, point-like source in the radio (Strom 1987), and discovery of radio pulses with an unusually fast 39.5-s period quickly followed (Kulkarni et al. 1988). Canonically, the pulsar's age and the estimated dynamical age of the SNR are consistent at $\sim 10^5$ yrs (Koo et al. 1990) and both have been determined to be at a distance of ~2.5 kpc. There is thus general agreement that the association is valid. Evidence for pulsed emission was subsequently found in γ-rays (Ramanamurthy et al. 1995) and possibly in X-rays (Safi-Harb et al. 1995; Chang & Ho 1997), with upper limits in the infrared (Clifton et al. 1988). The ROSAT observations in the X-ray regime do indicate a complex light curve strongly dominated by the intense X-ray radiation of a pulsar-powered synchrotron nebula (Safi-Harb et al. 1995; Becker & Truemper 1996). The unambiguous double-peaked γ-ray (EGRET) light curve obtained by Ramanamurthy et al. (1995) at the appropriate spin-down ephemeris suggested that the pulsar had a conversion efficiency, in terms of rotational energy to γ-rays, of ~0.004. Consequently there are strong grounds for the possibility of an optical detection.

However, the pulsar is quite distant and located within a rather complex SNR. Recent radio observations at 92 cm (Strom & Stappers 2000) indicate that the pulsar is located at the edge of the flat radio spectrum "core" of the SNR, and it is clear from X-ray observations that the pulsar is to some extent interacting with its environment. From models such as Pacini & Salvati (1987) and Shearer & Golden (2001) we would expect

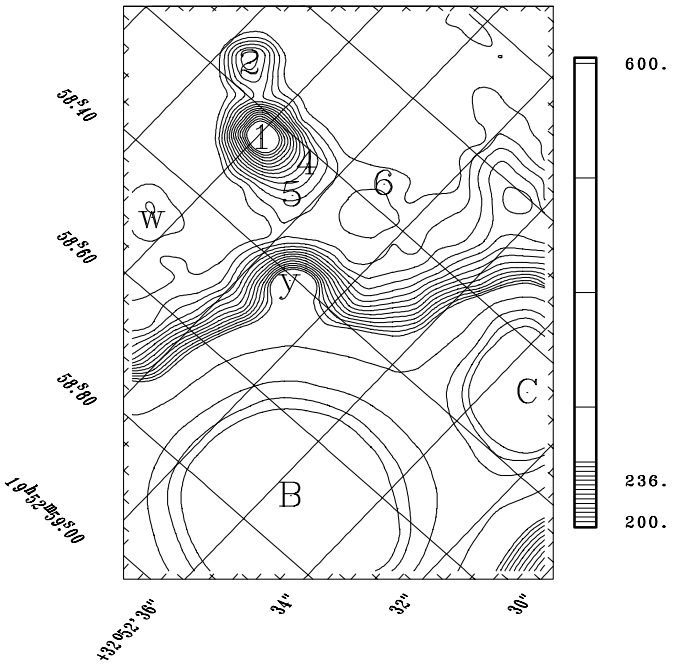

Fig. 1. Contour plot of the TRIFFID/MAMA V-band 8173-second summed image of the central region of CTB 80. This is a representation of the data first discussed by O'Sullivan et al. (1998); the image has been rotated and registered to the same coordinate system as the WFPC2 F547M image discussed in this paper. The main contours range from intensities of 200 to 252 in steps of 3 and were chosen to highlight the fainter structures. The pulsar optical counterpart candidates from Blair & Schild (1985), Fesen & Gull (1985), and O'Sullivan et al. (1998) are marked by their ID numbers (1, 2, 4, 5, 6). Other nearby detected stars are also marked (w, y). The bright stars identified as B and C by Blair & Schild (1985) are also marked and highlighted by a few extra contours between intensities of 300 and 600.

emission in the V magnitude range 24–26 depending upon the line of sight absorption, estimated from $E(B-V) = 0.8{-}1.4$ (Blair et al. 1984). Ground-based CCD observations by Blair & Schild (1985) and Fesen & Gull (1985) yielded a relatively crowded field with two possible counterparts at $m_V \sim 20$ and $m_V \sim 21$ respectively (known hereafter as counterparts 1 and 2).

Using a ground-based MAMA detector in the TRIFFID camera, we have previously examined the central field of CTB 80, but could find no evidence of pulsations in either B or V from these two counterparts (O'Sullivan et al. 1998). It was noted that counterpart 1 had an extension (see Fig. 1) towards the mapped radio timing position given in Table 2, which implied an unresolved stellar combination and/or plerionic/remnant material. Using PSF-fitting and deconvolution techniques, the removal of counterpart 1 yielded a best-estimate imposed decomposition of the "extension" into two further point sources (numbered 4 and 5 in Fig. 1), while a further point source (numbered 6 in Fig. 1) was detected some distance further away. These 3 sources had apparent magnitudes of $m_V \approx 22.1/B-V \approx 0.8$, $m_V \approx 22.6/B-V \approx 0.6$, and $m_V \approx 23.1/B-V \approx 0.0$. However, none of them exhibited pulsed emission at the 1% level. As was noted, both the photometry and time series analysis were complicated by their low signal-to-noise and proximity to counterpart 1.

It is clear that in order to unambiguously resolve the various apparent components within the radio error ellipse, diffraction-limited photometry must be obtained, which would facilitate further attempts to detect optical pulsations from the suspected optical counterpart(s) to PSR B1951+32. Consequently we obtained from the HST archive WFPC2 images of the CTB 80 SNR obtained with the F547W, F673N, F656N, and F502N passbands. In the next section we detail the reduction of the various exposures and their astrometric and photometric analyses. From this we assess the feasibility that we have identified new plausible optical counterparts, and assess the implications – both in terms of follow-up high speed 2-d photometry, and for current theoretical models.

Table 1. List of WFPC2 observations of the CTB 80 SNR, obtained from the ST-ECF HST archive.

Date (dd/mm/yy)	Filter Name	Total Exptime (seconds)	Notes
2/10/97	F656N	5300	H II
2/10/97	F673N	5400	S II
2/10/97	F502N	5400	O III
2/10/97	F547M	2600	Strömgren y

2. Analysis of archival HST/WFPC2 observations

We obtained from the HST archive all existing WFPC2 data of the CTB 80 SNR, as listed in Table 1. The core of the CTB 80 remnant lies on chip WF3 of the WFPC2 camera in every case. Image processing and photometry were performed using the IRAF (Tody 1993), STSDAS, and DAOPHOT-II (Stetson 1994) packages. The images in each band and chip were stacked and cleaned of cosmic rays and hot pixels using standard techniques. The F547M intermediate-width band enabled us to perform a deep photometric search for faint stellar sources, to $S/N = 2$ at $MAG_{\rm F547M} = 26.7$. Photometry was performed with DAOPHOT-II/allstar PSF-fitting, applying the correct "synthetic" zeropoint & gain ratio (Holtzman et al. 1995), correcting the photometry for CTE effects using the recipe of Stetson (1998), correcting for geometric distortion across the different WF chips, and correcting to the "standard" 0.″5 radius photometry.

2.1. The astrometric solution

Accurate mapping of the radio positions to the WFPC2 images requires a more precise astrometric plate solution than is provided in the WFPC2 image headers. The average absolute pointing error of HST is 0.″8 → 1.″5 (Biretta et al. 2000), due to errors in the Guide Star Catalog (GSC). Spacecraft roll can cause an additional shift of up to 1.″5. This degree of uncertainty, in this relatively crowded field, would make it impossible to pin down the identification of a probable optical counterpart to PSR B1951+32.

Therefore, using 31 stars on chip WF3 in common with the new 2MASS Point Source Catalog[1], and an iterative matching and fitting process, we derived a much improved astrometric solution with a total rms error of only 0.″15. The various published radio coordinates for PSR B1951+32 from the literature were filtered to yield only those which were judged to be fully independent of each other, and based either on genuine interferometric observations or on a timing solution which had not been affected by a glitch (although susceptible to timing noise). We list these two "best" radio positions for PSR B1951+32, from Foster et al. (1990) and Foster et al. (1994), in Table 2. Given that Migliazzo et al. (2002) have reported an accurate proper motion for the pulsar of 25 ± 4 mas yr^{-1} at PA $= 252°\pm7°$ from new VLA observations, the difference between the radio and HST epochs warranted a correction for significant proper motion. The 10.2 yr difference for the radio timing position resulted in a correction of 0.″254 in a WSW direction; the interferometric position was corrected by 0.″22 in the same direction, due to its 8.7 yr difference. The resulting positions (see Table 2) were then mapped onto the improved HST optical astrometric solution, and their corresponding 1-σ and 3-σ error ellipses are shown overplotting the F547M image in Fig. 2. As Foster et al. (1994) note, the discrepancy between them is probably the result of timing residuals, which may also lead to an underestimate of the errors for the timing result. This must be borne in mind when evaluating the nature of objects discovered optically in the vicinity of these radio positions.

2.2. A synchrotron nebulosity associated with PSR B1951+32

In Fig. 2, we note the presence of a patch of nebulosity $\sim$0.″8 $\times$ 1.″3 in extent, some or all of which lies within the mapped radio 3-σ error ellipses in the F547M image. It is not immediately evident in the narrowband images. As noted in Sect. 1, previous ground based time-resolved MAMA observations (O'Sullivan et al. 1998) have suggested the presence of such a broadband (present in both B and V) extended luminosity at this location. It was then assumed to be composed of two adjacent stars (numbered 4 and 5 in Fig. 1), but with the hindsight afforded by these higher resolution HST observations, we now know that "star" 4 marks the compact nebula, while "star" 5 is comprised of a blend of some of this nebula with some of star $4_{\rm HST}$ in Table 3. Leaving the source intact as a single compact nebula would have yielded photometry of $m_V \approx 21.6/B-V \approx 0.7$ in that MAMA data. After correction for reddening of $E(B-V) = 1.0$ (adopted from O'Sullivan et al. 1998), the colour of this nebula is $(B-V)_0 = -0.3\pm0.3$; clearly this is a blue object within the range of these wavebands. This colour is also consistent with the colours of synchrotron plerions associated with young pulsars – the Crab and PSR0540-69 in the LMC – with their approximately flat optical spectral indices.

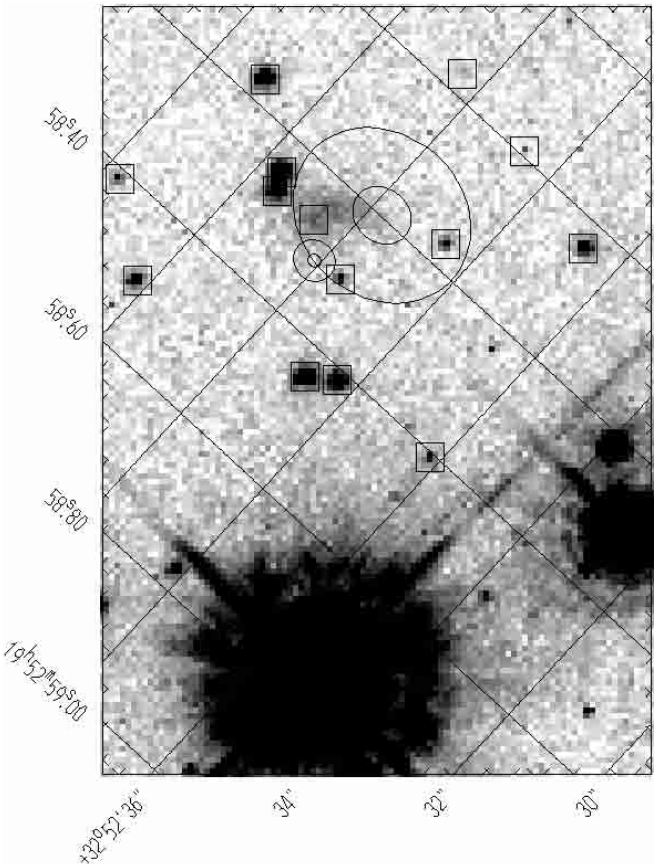

Fig. 2. Section of the WFPC2 F547M image, showing the same field and orientation as Fig. 1. The coordinate grid shows the improved astrometric calibration after referencing to the 2MASS point-source catalog. The mapped PM-corrected radio positions for PSR B1951+32 from Table 2 are marked by black ellipses, the semi-major and semi-minor axes of which are determined by the 1-σ and 3-σ total positional uncertainties in RA and Dec – i.e. the quoted error on the radio position, combined with the total rms error on the HST-2MASS fit for 31 stars. The larger pair of ellipses marks the interferometric position. The positions derived by DAOPHOT-II/allstar PSF-fitting for all measured point sources within 5.″0 of the centre of the synchrotron nebula are indicated by black squares.

2.3. Evidence for an optical counterpart to PSR B1951+32

Further evidence of the limits of ground-based observations of this field is seen in Fig. 2, where candidate 1 from Blair & Schild (1985) is itself resolved into 2 stars, $2_{\rm HST}$ and $3_{\rm HST}$, of roughly equal magnitude. Comparison with Fig. 1 shows that star 6 from O'Sullivan et al. (1998) is clearly recovered in this HST data as star $5_{\rm HST}$, as are the other nearby faint/crowded stars denoted "w" and "y" (the latter is also resolved into a close pair).

Now we turn our attention to the identification of candidates for an optical counterpart to PSR B1951+32. Five point-like sources were measured within or immediately outside the area covered by the larger 3-σ position ellipses. Of these, stars $1_{\rm HST}$ and $4_{\rm HST}$ are the most likely to be candidate counterparts. Both lie inside the 3-σ interferometric position ellipse, and although both lie outside the 3-σ timing position ellipse,

[1] 2MASS Second Incremental Data Release, 2000 March 2.

Table 2. Selected published radio coordinates for PSR B1951+32, which were used to determine its position on the WFPC2 F547M image. They are shown both in original form and corrected for proper motion to the 1997.753 epoch of the HST observations.

#	RA hh:mm:ss.sss	error s.sss	Dec dd:mm:ss.ss	error s.ss	Epoch	Equinox	Method	Reference
1	19:52:58.191	(0.038)	32:52:40.22	(0.56)	1989.03	J2000	Interferometry	Foster et al. (1990)
	19:52:58.174		32:52:40.15		1997.753	J2000		Foster et al. (1990) – PM corrected
2	19:52:58.3076	(0.0051)	32:52:40.569	(0.085)	1987.575	J2000	Timing	Foster et al. (1994)
	19:52:58.2886		+32:52:40.49		1997.753	J2000		Foster et al. (1994) – PM corrected

Table 3. The positions and magnitudes derived by DAOPHOT-II/allstar PSF-fitting for point sources detected in the WFPC2 F547M image of CTB 80. The "Dist." column contains the distance from from each source to the centre of the synchrotron nebula; only sources within 5.″0 of this position are listed here.

#	RA (2000) hh:mm:ss.ss	Dec (2000) dd:mm:ss.s	Dist. arcsec	MAG_{F547M} magnitudes
1_{HST}	19:52:58.24	32:52:41.0	0.20	24.26 ± 0.30
2_{HST}	19:52:58.25	32:52:41.8	0.97	22.49 ± 0.07
3_{HST}	19:52:58.23	32:52:42.0	1.11	21.69 ± 0.07
4_{HST}	19:52:58.28	32:52:39.9	1.16	24.54 ± 0.12
5_{HST}	19:52:58.14	32:52:39.0	2.23	24.41 ± 0.18
6_{HST}	19:52:58.14	32:52:43.4	2.69	22.18 ± 0.07
7_{HST}	19:52:58.42	32:52:39.2	2.90	21.96 ± 0.06
8_{HST}	19:52:58.39	32:52:38.7	2.95	22.30 ± 0.07
9_{HST}	19:52:58.48	32:52:42.6	3.55	23.33 ± 0.09
10_{HST}	19:52:57.95	32:52:40.8	3.57	26.06 ± 0.26
11_{HST}	19:52:58.39	32:52:44.1	3.73	24.59 ± 0.14
12_{HST}	19:52:57.97	32:52:39.1	3.79	26.20 ± 0.47
13_{HST}	19:52:58.02	32:52:37.1	4.68	23.24 ± 0.07
14_{HST}	19:52:58.38	32:52:36.6	4.74	24.77 ± 0.18

they are closer to it than any other sources. On the basis of position, neither is clearly a stronger candidate than the other. The difference between the two radio coordinates is primarily in Right Ascension – they are consistent with each other in Declination – which might indicate some systematic error in RA for one of these radio measurements. This would then favour the optical counterpart candidate which differed least in Dec from the two radio positions. However, both candidates lie roughly equidistant in Declination from a line connecting the two radio coordinates. The other possibility, as noted in Sect. 2.1, is that the entire error ellipse may be underestimated for the timing position; for example, a doubling of the axis lengths of this 3-σ ellipse would be just enough to make both candidates consistent with it.

Only one other measured source lies within the 3-σ interferometric position ellipse – star 5_{HST}, but this can be ruled out as a candidate counterpart because it is completely inconsistent with the radio timing position, even allowing for possible underestimated errors in the latter. Finally, the close pair of stars 2_{HST} and 3_{HST} lie just outside the 3-σ interferometric ellipse, and well outside the 3-σ timing position ellipse, which would be sufficient grounds for ruling them out as candidate counterparts; but two other factors rule them out with certainty: firstly they are too bright to be consistent with the emission predicted by the phenomenological models, and secondly they failed to exhibit optical pulsations in the study by O'Sullivan et al. (1998).

Of the two candidate counterparts, object 4_{HST} is a straightforward point-source measurement. However, object 1_{HST} requires some further analysis and comment. In *automatically* determining and fitting the list of stars detectable in the WFPC F547M image, this point-like source was detected within the small nebulous patch and measured at MAG_{F547M} = 24.3 ± 0.3 (ie. with a S/N of 3.1). Unfortunately, the narrow-band images were too insensitive to show such faint stellar sources, which therefore ruled out confirmation of the detection of this point-like source in another band. In Fig. 2, where we plot the F547M image superimposed with the detected point-like sources that survived our DAOPHOT-II/allstar analysis, it is clear that object 1_{HST} lies within the compact nebulosity which is unambiguously associated with the core of the CTB 80 SNR. It is also clear that this object is within the combined radio/optical error region for PSR B1951+32.

However, there is a problem with this photometric result for object 1_{HST}. An inspection of the resulting star-subtracted image shows that MAG_{F547M} = 24.3 must be an overestimation of the flux of the apparent point source within the nebula, as the fitting-and-subtraction process does not result in a smooth underlying background, but rather a pronounced "hole" in the nebula. This is a consequence of three probable factors: the undersampling of the WF3 PSF, coupled with the rapidly changing background in the vicinity of the source, and the possibility that the source is not a pure point-source but may be broadened by being embedded in a knot of the nebulosity.

To investigate this issue we performed the following test. The position of the source 1_{HST}, as determined by DAOPHOT-II/allstar, was kept constant, while its magnitude was varied from MAG_{F547M} = 21−29 in steps of 0.5 mag. At each magnitude it was subtracted from the original image and aperture photometry was performed on the resulting subtracted image, in order to measure the residual flux level within the central core pixels of the source. These residual fluxes were plotted as a ratio of the flux measured using the same aperture and background annulus on the original image; this ratio is an estimate

of the subtraction smoothness – see Fig. 3. In this figure, we also plot the median values and error bars for the same flux ratio of all the well-measured stars over the entire WF3 chip, binned in 0.5-mag intervals. For our pulsar counterpart candidate, one would expect to see subtraction smoothness of the same order as had been achieved for stars of the same brightness elsewhere in the field. The conclusion is that, to first order, the source would have to have $MAG_{\rm F547M} \geq 25.2$ to prevent *oversubtraction* into the nebula; and *undersubtraction* would occur at $MAG_{\rm F547M} \geq 26.2$. The magnitude of object $1_{\rm HST}$ therefore lies within this interval, but its S/N would be reduced to ≈2–2.5.

The question then arises, could one normally detect such a faint source as object $1_{\rm HST}$ in this data without these corrections, or is it spurious? We performed Monte Carlo simulations in order to test this hypothesis. Using the PSF shape and photometric zeropoint previously determined for the F547M image, artificial stars were added into the 512 × 512 pixel region centred on the nominal pulsar position. For each 0.5 mag step from $MAG_{\rm F547M} = 21-29$, 25 stars were added to this field at random positions, and then the same automatic star detection and measurement process was repeated in order to try to recover them. This entire process was repeated 100 times for robust statistics on the efficiency of star detection with increasing magnitude. Then, to take into account the effect of the higher background within the small nebula, which increases the sky noise, the simulations were repeated with the background everywhere increased to the mean background within the small nebula. The results are shown by the two traces in Fig. 4. Clearly, there is a good (between ≈60%–80%) probability of detecting a point source as faint as $MAG_{\rm F547M} = 25.5-26.5$. The *level* of the increased nebular background is shown to have only a very marginal effect on star detection (although the *gradients* within the nebular background are likely causes for bias in the photometric measurement, as has already been noted).

Crucially, the estimated magnitude of $MAG_{\rm F547M} = 25.2-26.2$ for object $1_{\rm HST}$, including the correction for the oversubtraction effect, is within the range predicted by the successful mode framework of Pacini & Salvati (1987) and more recently the phenomenological analysis of Shearer & Golden (2001). The magnitude of object $4_{\rm HST}$ is also consistent with these models, at the brighter end of the predicted range. Consequently, taken together with their positions with respect to the two radio-position error ellipses, we suggest that these two objects are plausible new optical counterpart candidates to PSR B1951+32. Both candidates lie within a region of area ≈1 arcsec^2. To estimate the probability of unrelated field stars being found within this region and at the same magnitude as the candidates, we computed a luminosity function (LF) for the total measured stellar content of the three near-identical WF chips – WF3 containing the pulsar field, and WF2 and WF4 abutting it and containing similar starfields. The LF was then normalised to give the density of foreground/background objects per arcsec^2 at 0.5-mag intervals. For object $4_{\rm HST}$ at $MAG_{\rm F547M} = 24.5$, the LF has over 300 stars or 0.02 stars per arcsec^2. For object $1_{\rm HST}$ at $MAG_{\rm F547M} \approx 25.75$, the LF has over 700 stars or 0.05 stars per arcsec^2. These numbers were not significantly increased when the LF was corrected for the corresponding detection efficiencies shown in Fig. 4. For the entire magnitude range of $MAG_{\rm F547M} = 24-26.5$, generously bracketing the two candidates and their uncertainties, the LF has over 3000 stars or 0.18 stars per arcsec^2. Thus the chance probability of finding two such objects an arcsecond apart is significant, but low.

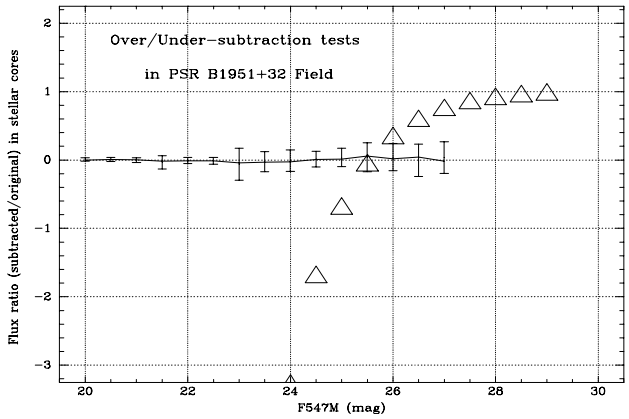

Fig. 3. Results of the star-subtraction tests to determine the magnitude range of the pulsar counterpart candidate $1_{\rm HST}$ wherein quantifiable over-subtraction or under-subtraction does not occur. Positive values of the flux ratio indicate under-subtraction (with +1 being essentially no subtraction at all), and negative values indicate over-subtraction. The triangular symbols denote the results for the pulsar counterpart candidate's test magnitudes. The line trace and error bars denote the median values and 1-σ errors of all the well-measured stars (those whose aperture photometry and PSF-fitting photometry agree to within ±0.5 mag) over the entire WF3 chip, binned in 0.5-mag intervals.

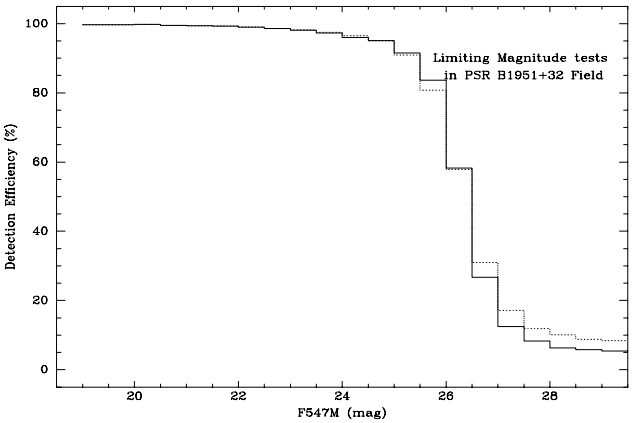

Fig. 4. Results of the Monte Carlo simulations for star detection/measurement probabilities in the 512×512 pixel region centred on the nominal pulsar position. The solid trace is for the original F547M image and the dotted trace is for the case of increased background. The background "detection" level seen here, at much fainter magnitudes than the realistic limiting magnitude cutoff, is due to the approximately 8% probability of "detecting" either noise peaks, or an *existing* star which happens to lie within the 2-pixel matching tolerance of an artificial star.

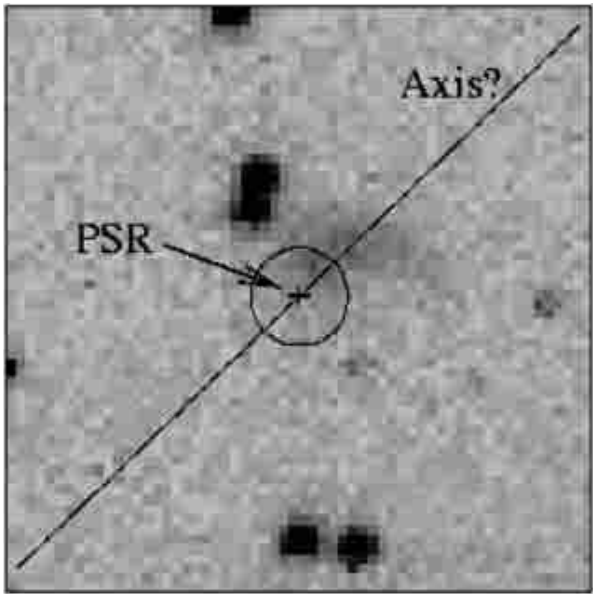

Fig. 5. Location of the radio counterpart according to Hester (2000b), along an axis that bisects apparent Balmer-dominated lobes (which lie outside the field shown here) in relation to the synchrotron nebula. Figure adopted from Hester (2000b).

3. Conclusions

Hester (2000a) has reported on a similar analysis of the same archival HST data, and agrees that the knot of extended continuum emission is synchrotron dominated as a consequence of the pulsar wind. Hester (2000b) places the radio counterpart 0.5″ to the East/SE of this nebula (see Fig. 5) – roughly between our proposed counterpart candidates 1_{HST} and 4_{HST}, although closer to 1_{HST} than to 4_{HST}. We have reproduced his results by mapping the Foster et al. (1994) radio timing position onto the *original* GSC-based astrometric solution from the HST data pipeline. However, we are more confident in our 2MASS-recalibrated astrometry, which also benefits from our correction utilising the accurate proper motion rate, published some time after Hester's analysis by Migliazzo et al. (2002). As a result our mapped radio timing position differs from Hester's by 0.″47. Hester also comments that the relative locations, orientation and luminosity are similar to the knot situated 0.5″ to the SE of the Crab pulsar. The agreement, in terms of synchrotron luminosity from the nebula, is compelling, regardless of which of the two astrometric solutions is used, since they overlap within their errors. However the location of the pulsar is still uncertain, given the considerable discrepancy between the two best independent radio positions. We have outlined the evolution in these radio positions and optical astrometric solutions which, taken together, locate the pulsar in an error region which is still too large to definitively pin down the pulsar's optical counterpart; however the more accurate mapped radio position (in terms of formal quoted errors) lies to the East/SE of the nebula. This supports the geometric orientation suggested by Hester (2000a,b).

One of the two newly resolved sources which we have identified as 1_{HST} and 4_{HST} may therefore indeed be the ∼24th–26th magnitude pulsar as predicted by the models of Pacini & Salvati (1987) and Shearer & Golden (2001). The other possibilities are that both are unrelated field stars, or that 1_{HST} is a localised "knot" within the bigger "knot" of the synchrotron nebula while 4_{HST} is a field star; both of these possibilities would imply that the true optical counterpart is fainter still. This would possibly reconcile one difficulty with the present analysis – the inconsistency of the two new candidates with the formally small error ellipse of the radio timing position; but it would create another difficulty – the inconsistency of candidates fainter than 26th magnitude with the phenomenological model predictions. Deeper HST and/or diffraction-limited adaptive optics imaging will be needed to determine which of these various possibilities is the correct interpretation, by putting some hard constraints on the colour and spectral index of both the synchrotron nebulosity and the candidate counterparts. Goldoni et al. (1995) noted that the optical spectral index *steepened* with age for the known optically emitting pulsars, while Shearer & Golden (2001) showed that this is consistent with the flattening of the pulse-peak luminosity relationship with the outer field strength. Consequently, with its expected steep optical spectral index, one would expect that the optical counterpart to PSR B1951+32 will not be as distinctly blue as younger Crab-like pulsars, but nevertheless distinguishable from regular thermally-emitting stars. Additionally, one could test the candidates by looking for proper motion, which (since the epoch of these HST observations) should now amount to a possibly detectable 0.″12. Follow-up timing studies with the upgraded TRIFFID imaging photon-counting camera would permit the search for optical pulsations from a securely identified counterpart, with much higher statistical significance than previously. Not only would this provide the essential confirmation of any optical counterpart, it would also test the hitherto successful optical models of Pacini & Salvati (1987) and Shearer & Golden (2001) in an age regime where few optical pulsars have been found.

Acknowledgements. The authors gratefully acknowledge financial support from Enterprise Ireland under the Basic Research Programme. RFB is also grateful for financial support from the Improving Human Potential programme of the European Commission (contract HPFM-CT-2000-00652). This publication is based upon Hubble Space Telescope data obtained from the ST-ECF archive, ESO, Garching, Germany. It also makes use of data products from the Two Micron All Sky Survey, which is a joint project of the University of Massachusetts and the Infrared Processing and Analysis Center/California Institute of Technology, funded by the National Aeronautics and Space Administration and the National Science Foundation. Finally, we also wish to thank the referee, Richard Strom, for his useful suggestions and constructive comments which have considerably improved the paper's content and presentation.

References

Becker, W., & Truemper, J. 1996, A&AS, 120, 69
Biretta, J. A., et al. 2000, WFPC2 Instrument Handbook, Version 5.0 (Baltimore: STScI)
Blair, W. P., Kirshner, R. P., Fesen, R. A., & Gull, T. R. 1984, ApJ, 282, 161
Blair, W. P., & Schild, R. E. 1985, ApL, 24, 189
Chang, H.-K., & Ho, C. 1997, ApJ, 479, L125

Clifton, T. R., Backer, D. C., Neugebauer, G., et al. 1988, A&A, 191, L7
Daugherty, J. K., & Harding, A. K. 1996, A&AS, 120, 107
Fesen, R. A., & Gull, T. R. 1985, ApL, 24, 197
Foster, R. S., Backer, D. C., & Wolszczan, A. 1990, ApJ, 356, 243
Foster, R. S., Lyne, A. G., Shemar, S. L., & Backer, D. C. 1994, AJ, 108, 175
Goldoni, P., Musso, C., Caraveo, P. A., & Bignami, G. F. 1995, A&A, 298, 535
Hester, J. 2000a, AAS, 197, 8216
Hester, J. 2000b, in Spin and Magnetism in Young Neutron Stars, conference, Institute for Theoretical Physics, UC Santa Barbara
Holtzman, J., Burrows, C., Casertano, S., et al. 1995, PASP, 107, 1065
Koo, B.-C., Reach, W. T., Heiles, C., Fesen, R. A., & Shull, J. M. 1990, ApJ, 364, 178
Kulkarni, S. R., Clifton, T. C., Backer, D. C., Foster, R. S., & Fruchter, A. S. 1988, Nature, 331, 50
Migliazzo, J. M., Gaensler, B. M., Backer, D. C., et al. 2002, ApJ, 567, L141
O'Sullivan, C., Shearer, A., Colhoun, M., et al. 1998, A&A, 335, 991
Pacini, F., & Salvati, M. 1987, ApJ, 321, 447
Ramanamurthy, P. V., et al. 1995, ApJ, 447, L109
Romani, R. W. 1996, ApJ, 470, 469
Safi-Harb, A., Ögelman, H., & Finley, J. P. 1995, ApJ, 439, 722
Shearer, A., & Golden, A. 2001, ApJ, 547, 967
Stetson, P. B. 1994, PASP, 106, 250
Stetson, P. 1998, PASP, 110, 1448
Strom, R. G. 1987, ApJ, 319, L103
Strom, R. G., & Stappers, B. W. 2000, IAU Colloq. 177: Pulsar Astronomy - 2000 and Beyond, ASP Conf. Ser., 202, 509
Tody, D. 1993, Astronomical Data Analysis Software and Systems II, ed. R. J. Hanisch, R. J. V. Brissenden, & J. Barnes, ASP Conf. Ser., 52, 173